Physicochem. Probl. Miner. Process., 59(3), 2023, 168454

http://www.journalssystem.com/ppmp

Physicochemical Problems of Mineral Processing

ISSN 1643-1049

The depression mechanism on pyrite in a low-alkaline system with combined depressants: Experiment, HSC, DFT and ToF–SIMS studies

Suqi Li [1], Jiaqiao Yuan [1], Zhan Ding [1], Jie Li [1], Anmei Yu [1], Shuming Wen [1,2,3], Shaojun Bai[1,2,3]

[1] Faculty of Land Resource Engineering, Kunming University of Science and Technology, Kunming 650093, Yunnan, China

[2] State Key Laboratory of Complex Nonferrous Metal Resources Clean Utilization, Kunming University of Science and Technology, Kunming 650093, China

[3] Yunnan Key Laboratory of Green Separation and Enrichment of Strategic Mineral Resources, Kunming 650093, China

Corresponding author: baishaojun830829@126.com (Shaojun Bai)

Abstract: Depression of pyrite in a low-alkaline system has sparked soaring interests for the multi-metal sulfide minerals flotation recently. This study investigates effects of combined depressants ($Ca(ClO)_2$ and CaO) on pyrite flotation with butyl xanthate (KBX). Micro-flotation experiments indicate that the addition of 200 mg/L combined depressants (a mass ratio of CaO to $Ca(ClO)_2$ of 2:3) and 1.0×10^{-3} mol/L KBX at pH 9.5 can effectively depresses the flotation of pyrite, and a minimum pyrite recovery rate of 12.5% is obtained. Basic thermodynamic evaluation results confirm the participation of $Ca(ClO)_2$ significantly decrease the negative Gibbs free energies of pyrite oxidation reaction. Besides, the calcium species ($Ca(OH)_2$, Ca^{2+} and $Ca(Cl)_2$) will spontaneously transform into $CaCO_3$,and it is the ultimate dominant calcium species in the CO_3^{2-} system. Density functional theory (DFT) results indicate that $CaCO_3$ can chemically adsorb onto the pyrite surface with an adsorption energy of –671.13 kJ/mol. The O1 and Ca atoms mainly contribute to the bonding process and are responsible for the stable adsorption of $CaCO_3$. ToF-SIMS results provide strong evidence that the combined depressants increase the amount of hydrophilic species and decrease dixanthogen adsorption onto the pyrite surface. The thickness of the whole formed hydrophilic species is approximately 50 nm. Semiquantitative amounts of hydrophilic species follow the order of hydroxy calcium>iron carbonyl>calcium carbonate. Overall, hydrophilic species repulse adsorption of dixanthogen and significantly reduce the flotation performance of pyrite.

Keywords: pyrite, calcium hypochlorite, lime, depression, low alkaline system

1. Introduction

Pyrite (FeS_2) is the most ubiquitous metal sulfide mineral in nature. Usually, it is associated with valuable sulfide minerals such as chalcopyrite, galena, and sphalerite (Bonnissel-Gissinger et al., 1998; Chandra and Gerson, 2010; Janetski et al., 1977; López Valdivieso et al., 2004; Mu et al., 2016b; Wang et al., 2015). Although pyrite can be served as an important industrial raw material for sulfuric acid production, it often needs to be ideally depressed with the aims of separation from other valuable sulfide minerals through froth flotation. To date, the selective flotation separation of pyrite faces many challenges in practice (Bai et al., 2019). On the one hand, metal sulfide minerals possess similar floatability, and partial recovery of pyrite can be obtained even the pyrite is subjected to depress in alkaline pulp systems (7.5–11) (Guo et al., 2016; Wang and Forssberg, 2002). On the other hand, unavoidable metallic ions, such as Cu^{2+} and Pb^{2+},commonly exist in the flotation pulp, which will lead to the unintentional activation of pyrite (Bai et al., 2013; Barker et al., 2014; Deng et al., 2013; Dichmann and Finch, 2001; EkmekcI and Demirel, 1997; Finkelstein, 1997; Pecina et al., 2006; Peng et al., 2012). As a result, pyrite easily floats to the concentrate and dilutes concentrate grades (Huang et al., 2013). The interfusion of pyrite inevitably increases smelting costs and causes potential environmental pollution during following basic metal extraction (Ahmadi et al., 2012; Bulut et al., 2014). Thus, the depression of pyrite during the complex sulfide ore flotation is vital for economic and environmental perspectives.

DOI: 10.37190/ppmp/168454

In flotation plants, the rejection of pyrite mostly relies on the aids of various depressants. At present, multitude depressants have been studied to regulate the flotation behaviour of pyrite during the multi-metal sulfide minerals beneficiation. It mainly includes inorganic depressants, organic depressants and two or more of combination (Mu et al., 2016a, 2016b). Among of them, lime (CaO), as an inorganic depressant exhibits relatively superior inhibition effects on pyrite in a high alkali lime craft (at extremely high pH>11) (Ding et al., 2022). This is stemmed from the fact that the lime promotes the formation of hydrophilic iron hydroxyl and calcium species on pyrite surfaces and hinders the adsorption of collectors (Chen et al., 2011; Jin et al., 2018; Li et al., 2012). Whereas, the high alkali lime craft causes some problems in industry. For instance, the flotation selectivity of sulfide minerals becomes worse, and flotation recovery rate of valuable sulfide minerals decreases in the extremely high alkali pulp (Zanin et al., 2019). Besides, a large amount of lime addition will cause pipe blockage, and influence the plant operation (Shen et al., 1998). Hence, depression of pyrite in a low-alkaline medium is urgent and has sparked soaring interests for the multi-metal sulfide minerals flotation.

At present, many researches have been conducted on the selective depression of pyrite in the low-alkaline medium via surface oxidation due to the advantages of simple operation and feeble influence to the environment. The oxidants widely applied for selective depression of pyrite involve hydrogen peroxide (H_2O_2) (Khoso et al., 2019), hypochlorite (NaClO, $Ca(ClO)_2$) (Bai et al., 2019; Liu et al., 2015; Yin et al., 2019), ferrate (K_2FeO_4 or Na_2FeO_4) (Liao et al., 2022), potassium permanganate ($KMnO_4$) (Zhang et al., 2022) and ozone (O_3) (Khoso et al., 2019). Among of them, $Ca(ClO)_2$ is a promising depressant for pyrite differential flotation of base metal sulfide ores. Ai et al. indicated that the pyrite was depressed desirably at a low alkalinity of pH 7–8 with addition of $Ca(ClO)_2$+DT-2# based on pure mineral experiments (Ai et al., 2015). Yin et al. studied the effect of $Ca(ClO)_2$ on the flotation separation of covellite and pyrite with ammonium dibutyl dithiophosphate at pH 10 (Yin et al., 2019). Results demonstrated that the adsorption of $Ca(OH)^+$, $CaSO_4$, and $Fe(OH)_3$ caused by the oxidization of $Ca(ClO)_2$ was responsible for the pyrite depression. Recently, we investigated effects of $Ca(ClO)_2$ on the pyrite flotation under low alkaline conditions (pH=8.5). The results showed that $Ca(ClO)_2$ promoted the pyrite surface to form multitude hydrophilic substances, and improved the hydrophilicity of pyrite significantly. However, the pyrite recovery still reached approximately 30% under the recommended conditions (Bai et al., 2019). To sum up, $Ca(ClO)_2$ played an important role in the pyrite depression. Whereas, the improvements in depression efficiency and selectivity are needed to receive further study. Moreover, the underlying mechanism behind that should be further discussed. Motivated by these observations, depression of pyrite in a low-alkaline system with the addition of combines depressants ($Ca(ClO)_2$ and CaO) was performed.

In this work, micro flotation experiments, basic thermodynamic evaluation and computational methods were conducted to investigate the depressant mechanism of combines depressants on pyrite with KBX in a low-alkaline system. In addition, Time-of-Flight Secondary Ion Mass Spectrometry (ToF-SIMS) was used to characterize the surfaces of the pyrite and provide strong evidence for specific variations of hydrophily and hydrophobicity of mineral surfaces. This study provided valuable insights into the calcium hypochlorite oxidation modification of the pyrite surface and its response to flotation behavior, and thus presented a fundamental understanding on the selective flotation separation of pyrite from other sulfide minerals.

2. Experimental methods

2.1. Material and regents

The pure mineral samples of pyrite studied in this work were obtained from Yunnan, China. Firstly, the selected high-purity samples were finely ground in an agate mortar after manual crushing and hand-picking. Then, a certain amount of -74+38 μm pyrite samples were acquired by dry screening, and stored under the vacuum condition to prevent surface oxidation of mineral. The chemical composition of the pyrite samples was analyzed, and the results confirmed that the purity of the pyrite samples was over 95%, of which the Fe content was 45.39% and the S content was 52.58%. Additionally, the pyrite sample was further analyzed by X-ray diffraction (XRD) and only the signal from pyrite was observed (Fig. 1).

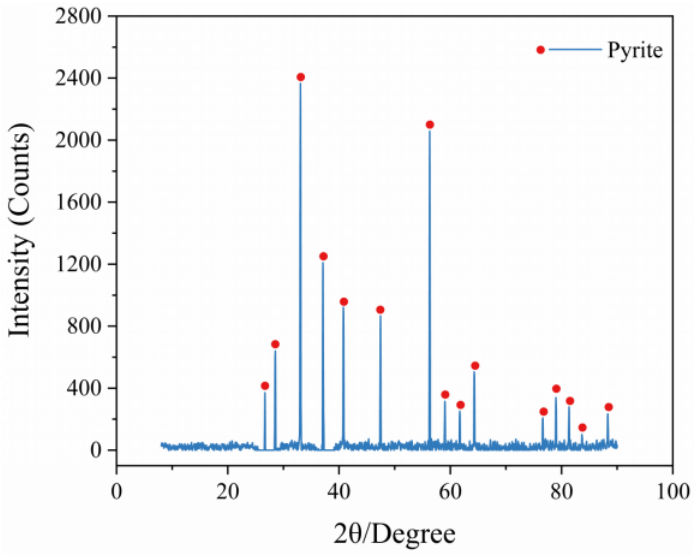

Fig.1. X-ray diffractograms of pyrite samples

NaOH, Na_2CO_3 and HCl (analytical grade, Shanghai chemical) were used as pH regulator in this works. It is worth noting that Na_2CO_3 was served as regulator for the medium and low alkalinity pulp (pH=7-10), while NaOH was used to regulate the high alkalinity pulp (pH>10). Calcium hypochlorite ($Ca(ClO)_2$, analytical grade, Tianjin chemical) and lime (CaO, analytical grade, Tianjin chemical) were used to prepare the combined depressants. KBX ($C_5H_{11}OS_2K$, commercial grade, Zhuzhou chemical) was used as the collector. Terpenic oil ($C_{10}H_{17}OH$, commercial grade, Zhuzhou chemical) was served as the frother. All solutions were prepared with deionized (DI) water (resistivity 1.8×10^7 Ω•cm) purified by a Milli-Q5O system (Billerica, MA, USA).

2.2. Methods and apparatus

2.2.1. Micro-flotation experiments

Pure pyrite flotation experiments were conducted in a flotation cell (XFG-type, Wuhan). 2.0 g of pyrite sample was mixed with 40 mL of deionized water in the flotation cell to create a pulp density of ~5% for stirring 2 min at 900 rpm with a specific air flow. Then, the pH adjuster was added to the pulp and conditioned for 2 min. Afterward, combined depressants (if present) were added with 4 min of conditioning. Finally, KBX and pine oil were added respectively, and the pulp was conditioned for 2 min with each reagent. The flotation time was fixed for 4 min at room temperature. Recovery of the concentrate, which was calculated based on the rate of froth products weight to raw ore weight was treated as responses to evaluate the flotation index.

2.2.2. Basic thermodynamic evaluation

For the thermodynamic analysis of the process, HSC Chemistry version 3.0 was used to calculate the Delta G-T diagrams for the involved reactions. These thermodynamic considerations provided important information for the chemical reaction tendency, the stability and the equilibrium amount of the reaction products, which could reveal the mechanisms of pyrite depression in different oxidation systems.

2.2.3. Computational methods

The interaction mechanism of H_2O-$CaCO_3$ with the pyrite surface was investigated with the Cambridge Serial Total Energy Package program in Materials Studio 2017 (Bunkholt and Kleiv, 2015; Wang et al., 2021). The DFT plane-wave pseudopotential method was used to investigate the various properties and geometry of the adsorbate and the surface systems (Mkhonto et al., 2022; Zhang et al., 2023). The generalized gradient approximation (GGA) using the Perdew, Burke, and Ernzerhof (PBE) functional

was employed for the exchange–correlation functional (Zhang et al., 2023). The interaction between the ionic core and valence electrons was described by ultrasoft pseudopotentials (Zhang et al., 2023). We employed the plane wave cut-off energies of 330 eV. These demonstrated convergence for the bulk models to within 0.2 meV/atom. Brillouin-zone integration was performed with a 2 × 3 × 1 k-point mesh for all of the calculations. For self-consistent electronic minimization, the Pulay Density Mixing Method was employed at a convergence tolerance of 2.0×10^{-6} eV/atom. The convergence criteria for structure optimization and energy calculation were set to (a) an energy tolerance of 1.0×10^{-6} eV/atom, (b) a maximum force tolerance of 0.03 eV/Å and (c) a maximum displacement tolerance of 0.001 Å.

Based on the XRD results (Fig.1), the pyrite (FeS_2) was defined with space group symmetry of Pa-3. The relaxed unit cell of the bulk structure was found to have lattice vectors of a=b=c =5.413 Å, and α=β=γ=90°, which was very close to the experimental lattice vectors of pyrite (Ferreira et al., 2021). Additionally, the pyrite (100) surface was selected to calculate the properties and adsorption energies because (100) surface of the pyrite crystal is the most stable and has the lowest energy (Hung et al., 2002; Mkhonto et al., 2022; Shen et al., 1998). The adsorption energies of H_2O-$CaCO_3$ on the pyrite (100) surface were calculated using the following equations (Mkhonto et al., 2022):

$$\Delta E_{ads}=E_{total}-\left(E_{surf}+E_{H_2O}+E_{CaCO_3}\right) \quad (1)$$

where ΔE_{ads} is the adsorption energies of H_2O and $CaCO_3$ on the pyrite (100) surface, E_{total} is the total energies of H_2O-$CaCO_3$ after adsorption on the pyrite (100) surface, E_{surf} is the energy of isolated pyrite surface, while E_{H_2O} and E_{CaCO_3} are the energies H_2O and $CaCO_3$, respectively.

2.2.4. Time-of-flight secondary ion mass spectroscopy (ToF-SIMS) measurements

The characterizations of pyrite surface before and after the combined depressants and KBX treatments were accomplished by the ToF-SIMS V (ION-TOF GmbH, Münster, Germany). The primary ion beam of 15 keV Bi^{3+} was operated in a static mode with a primary pulsed beam current of 0.5 pA. The area of each sample for spectral acquisition was 100×100 μm². The sputter ion of 500 kV Cs was used with a sputter current of 51 nA, and the sputter area was 300×300 μm². Positive ion spectra were collected from each individual region of interest (ROI). Three ROIs were investigated on the samples to obtain statistically significant results. Prior to statistical analysis, the intensities of the prominent secondary ions in the ToF-SIMS spectra were normalized to the total ion yield. The analysis was conducted in a vacuum on the order of 10^{-9} Pa.

Powder pyrite samples were used for the ToF-SIMS analysis of normalized peak intensities to investigate the effect of combined depressants on pyrite surface properties, as well as on the adsorption of the collector KBX. 2 g pyrite (−74 + 38 μm) was mixed with 40 mL of DI water in the flotation cell for stirring 2 min at 900 rpm with 0.9 L/min air flow. Na_2CO_3 was added to maintain the pH at 9.5. Then, 200 mg/L of combined depressants (a mass ratio of CaO to $Ca(ClO)_2$ of 2:3) was added to the cell with 4 min of conditioning. Afterward, KBX (1×10^{-3} mol/L) were added, and the pulp was conditioned for 15 min. Finally, the samples were removed, repeatedly rinsed with a pH 9.5 solution and then filtered and dried. Besides, the pyrite sample with a same treatment process as the above-mentioned (Note: no addition of the combined depressants) was analyzed to allow for contrast testing. Additionally, freshly fractured pyrite samples were used for ToF-SIMS depth profiling, and the treatment process was same to that of powder pyrite samples. The ToF-SIMS spectral acquisition was conducted within 24 h of the sample preparation.

3. Results and discussion

3.1. Review of micro-flotation test results

The pyrite recovery as a function of pH in the absence and presence of combined depressants was shown in Fig.2. Flotation conditions were as follows: the dosage of combined depressants was 150 mg/L with a mass ratio of CaO to $Ca(ClO)_2$ of 2:3, the KBX collector was 1×10^{-3} mol/L and the air flow was 0.5 L/min. From Fig. 2, pyrite displayed desirable floatability at the pH range of 5.5–11.2 in the absence of combined depressants, and the pyrite recovery ranged from 75.5% to 91.5%. A further increase in the pH to 13, the pyrite recovery decreased sharply (54.2%). This phenomenon was caused by the suppression of OH^- ions stemming from the high-alkaline systems (Zhao et al., 2023). Nevertheless, the

influences of pH on pyrite flotation were less obvious in the presence of combined depressants, and the concentrate recovery decreased from 42.5% to 22.5% when the pH increased from 5.5 to 9.5. Meanwhile, the variation in the concentrate recovery was small as the pH increased further. The recommended test pH is 9.5, and the maximum concentrate recovery difference (65.1%) between pyrite and depressed-pyrite was observed. Herein, the addition of combined depressants in a low-alkaline system could effectively depress the pyrite and hopefully created favorable conditions for the flotation separation of pyrite from other sulfide ores.

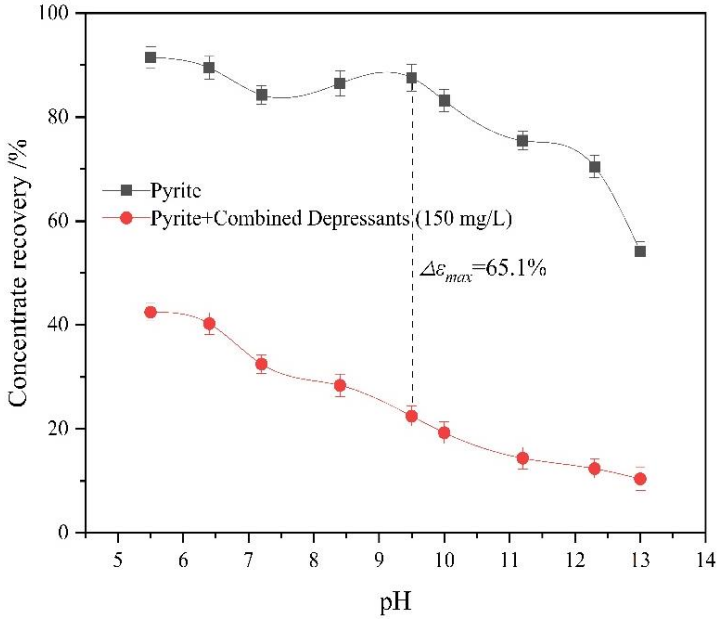

Fig. 2. Effects of pH on the pyrite flotation. Conditions: the dosage of combined depressants was 150 mg/L with a mass ratio of CaO to $Ca(ClO)_2$ of 2:3, the KBX collector was 1×10^{-3} mol/L and the air flow was 0.5 L/min at room temperature

Fig. 3 presented the influence of combined depressants (a mass ratio of CaO to $Ca(ClO)_2$ of 2:3) dosage on the pyrite recovery in the presence of 1×10^{-3} mol/L KBX collector at pH 9.5 and an air flow of 0.5 L/min. As shown in Fig. 3, the combined depressants provided an easy access to the pyrite depression. The concentrate recovery decreased rapidly with the increase in the combined depressants dosage (50 -175 mg/L); it was only 13.5% when a combined depressant dosage of 200 mg/L was added. With a further increase in combined depressant dosage, a minimal change in the concentrate recovery was observed. It was possible that multitude of hydrophilic species were generated on the pyrite surfaces due to the strong oxidation of $Ca(ClO)_2$, as well as the adsorption of calcium components in a low-alkaline system. This behavior reduced collector adsorption, resulting in the serious depression of pyrite.

The pyrite recovery rates with different mass ratios of CaO to $Ca(ClO)_2$ at pH 9.5 were shown in Fig.4. The dosage of combined depressants was 200 mg/L, the KBX collector was 1×10^{-3} mol/L and the air flow was 0.5 L/min. As illustrated in Fig.4, the pyrite recovery rates decreased as the mass ratios of CaO to $Ca(ClO)_2$ decreased with the ratios range of 1:0–2:3. Specially, the pyrite recovery rate reached 37.5% when the mass ratios of CaO to $Ca(ClO)_2$ was 1:0 (equal to 200 mg/L of CaO), while a minimum pyrite recovery rate with 12.5% was obtained when the mass ratios of CaO to $Ca(ClO)_2$ was 2:3. The results confirmed that the increase of $Ca(ClO)_2$ dosage in the combined depressants was conducive to the pyrite depression, and the addition of single lime failed to depress the pyrite effectively in the low-alkaline system. Notedly, the pyrite recovery presented uptrend (16.7%) when the mass ratios of CaO to $Ca(ClO)_2$ was 0:1 (equal to 200 mg/L of $Ca(ClO)_2$). We inferred that the single lime with shortage dosage led to the unsatisfactory inhibition effect of pyrite, while $Ca(ClO)_2$ could promote the formation of multitude hydrophilic species on the pyrite surfaces. Given these results, the combined usage of CaO and $Ca(ClO)_2$ facilitated the pyrite depression, and the presence of $Ca(ClO)_2$ exhibited more important role in this behavior. Thus, the recommended mass ratios of CaO to $Ca(ClO)_2$ was 2:3.

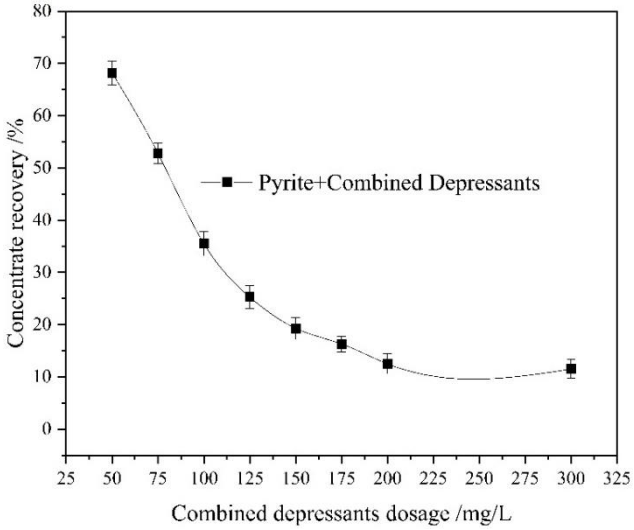

Fig. 3. Effects of combined depressants dosage on the pyrite flotation. Conditions: pH=9.5, the mass ratio of CaO to $Ca(ClO)_2$ was 2:3, the KBX collector was 1×10^{-3} mol/L and the air flow was 0.5 L/min at room temperature

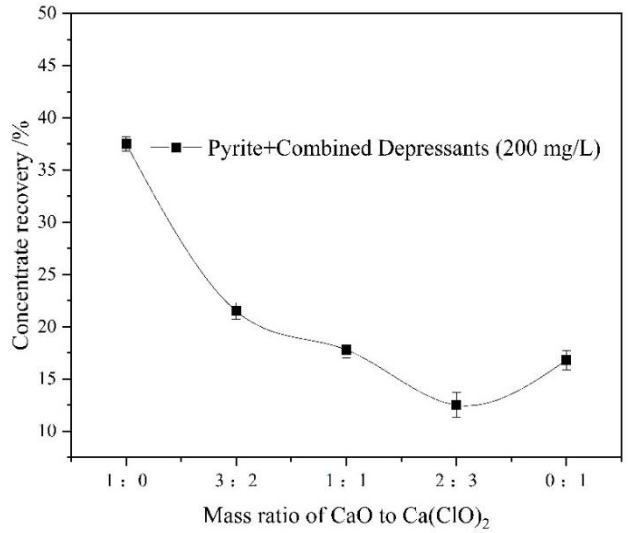

Fig. 4. Effects of mass ratio of CaO to $Ca(ClO)_2$ on the pyrite flotation. Conditions: pH=9.5, the dosage of combined depressants was 200 mg/L, the KBX collector was 1×10^{-3} mol/L and the air flow was 0.5 L/min at room temperature

Fig. 5 showed the effect of air flow on the flotation performance of pyrite at pH 9.5 with a KBX collector dosage of 1.0×10^{-3} mol/L and the combined depressants dosage of 200 mg/L (a mass ratio of CaO to $Ca(ClO)_2$ of 2:3). As depicted in Fig. 5, the pyrite recovery rate decreased from 33.8% to 9.13% when the air flow increased from 0 to 0.9 L/min. The result indicated the influx of air reinforced the pyrite oxidation and improved the hydrophilicity of the pyrite surface, which was consistent with the previous research result (Jiang et al., 2023). Hence, the recommended air flow was 0.9 L/min. Obviously, the combined effects of air flow and the depressants played important roles in the pyrite depression on the basis of the review of micro-flotation test results. The corresponding depression mechanism on pyrite in a low-alkaline system will be discussed in following sections.

3.2. Thermodynamic calculation results

3.2.1 Pyrite oxidation reaction in different system

The thermodynamic calculation of the pyrite oxidation reaction in different system was performed

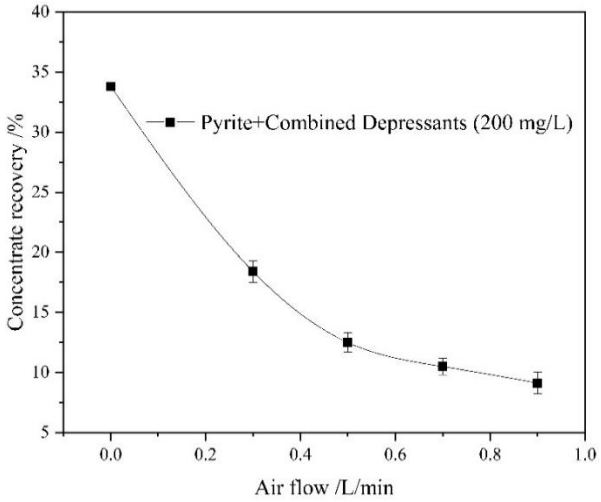

Fig. 5. Effects of air flow on the pyrite flotation. Conditions: pH=9.5, the dosage of combined depressants was 200 mg/L with a mass ratio of CaO to $Ca(ClO)_2$ of 2:3, and the KBX collector was 1×10^{-3} mol/L at room temperature.

using the HSC Chemistry version 3.0 software, and the results were shown in Fig. 6. As can be seen, the oxidation reaction of pyrite in the H_2O system at the temperature of 0-40 °C failed to occur spontaneously due to their positive Gibbs free energies (Fig. 6 (a)). Whereas, the oxidation reaction of pyrite in the presence of O_2 occurred spontaneously, giving birth to the formation of S^0, $FeSO_4$, Fe_2O_3 or Fe_3O_4 (Fig. 6 (b)). It is well accepted that the formation of hydrophobic S^0 has benefits for the pyrite flotation, whereas the generation of hydrophilic iron oxide ($FeSO_4$, Fe_2O_3 or Fe_3O_4) depresses the pyrite (Bai et al., 2021). Thus, increasing the oxygen amount will increase the hydrophilicity of the pyrite surface, which explain the decrease in the pyrite recovery with the increase of air flow (as depicted in Fig. 5). In the H_2O-O_2 system, sulfur components in pyrite were preferentially converted to SO_4^{2-} ions,

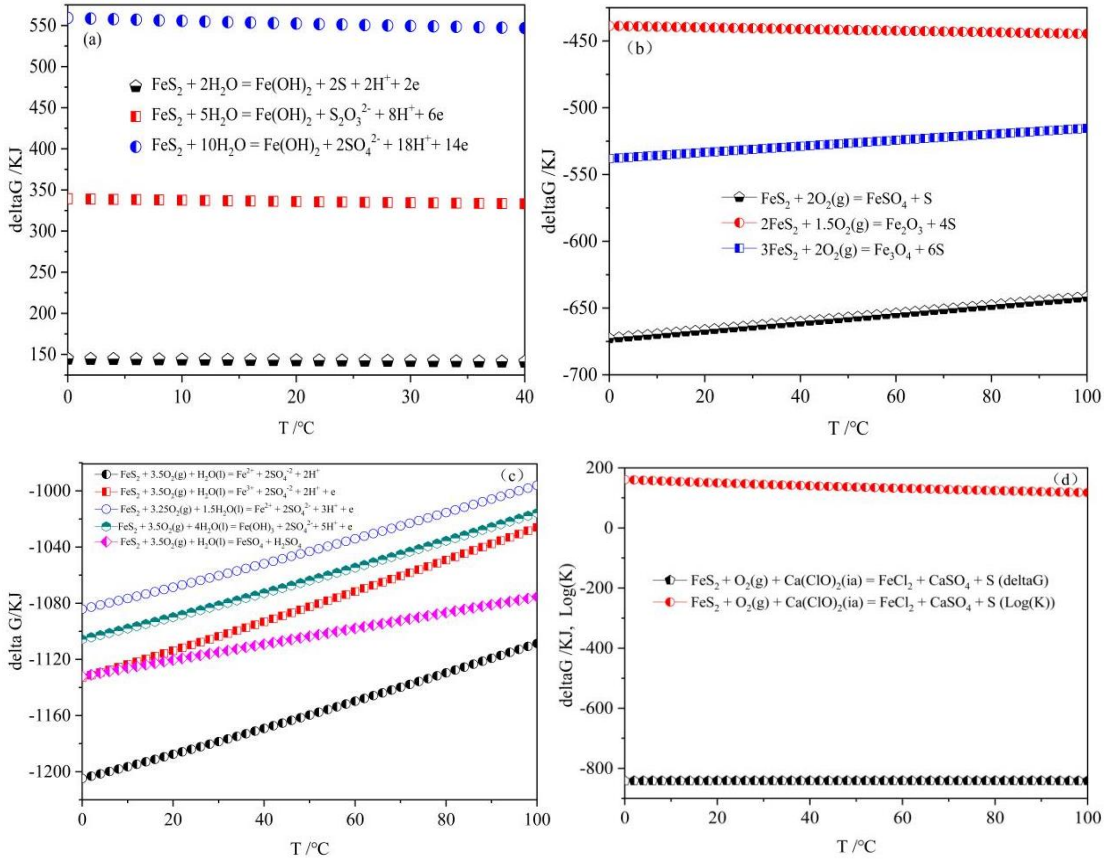

Fig. 6. Relationships between the Gibbs free energy of pyrite oxidation reaction and temperature

while iron components were preferentially converted to Fe^{2+} ions during the pyrite oxidation processing because of its lower Gibbs free energy (Fig. 6 (c)). Besides, the iron components in the pyrite could convert to $Fe(OH)_3$ spontaneously as the oxidation reaction continued, which was an important hydrophilic species for the pyrite depression.

The oxidation reaction of $Fe_2S + O_2 + Ca(ClO)_2 \rightarrow FeCl_2 + CaSO_4 + S$ occurred spontaneously due to the negative Gibbs free energies, and the large reaction constant (Fig. 6 (d)). Moreover, the pyrite oxidation reaction exhibited larger spontaneous tendency with the participation of $Ca(ClO)_2$ comparing with spontaneous tendency of corresponding oxidation reaction with single O_2 participation (Fig. 6 (b)). It was possible that water participated in the mineral surface oxidation process, decreased the energy barrier of the reaction, and thus promoted the oxidation process.

To further investigate the effect of oxygen dosage on the pyrite oxidation products, the relationship between the equilibrium amounts of pyrite oxidation products and oxygen dosage was analysed. As shown in Fig. 7, the pyrite content decreased linearly with the increase of oxygen dosage from 0 to 4 mole, and the pyrite constantly converted to S^0 and $FeSO_4$. With a further increase in the oxygen dosage, the S^0 and $FeSO_4$ converted to $Fe_2(SO_4)_3$, SO_2 and SO_3. Thus. the amount of oxygen reactant determined the specific oxidation products of pyrite, which considerably affected the hydrophilic or hydrophobic characteristics of the pyrite. Obviously, a deepness oxidation caused by oxygen would promote the formation of hydrophilic iron oxide on the pyrite surfaces, and facilitated the pyrite depression.

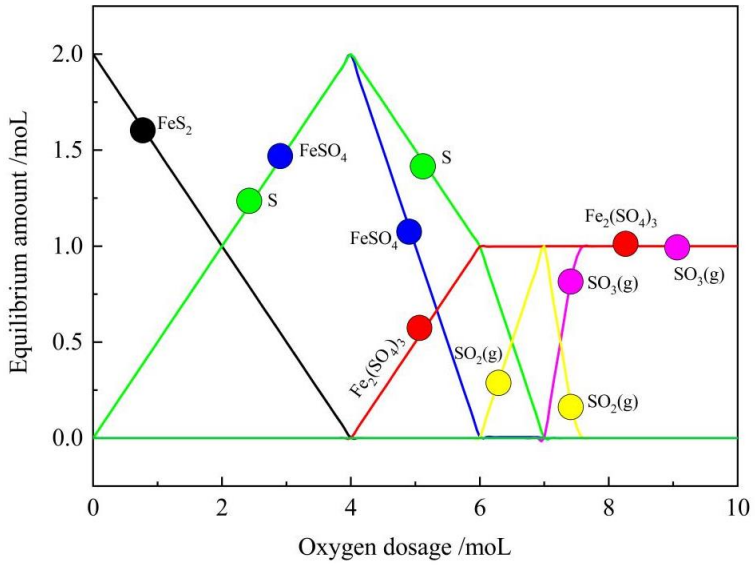

Fig. 7. Relationships between the equilibrium amounts of pyrite oxidation products and oxygen dosage

3.2.2. Calcium species transformation reaction

Fig. 8 showed the Gibbs free energy change as a function of temperature for calcium species transformation reactions. Results indicated that decomposition reactions of $Ca(ClO)_2$ were inevitable at the temperature range of 0-100 °C because of their negative Gibbs free energies. Meanwhile, the decomposition reaction of $Ca(ClO)_2 + OH^- \rightarrow Ca(OH)_2 + 2Cl^- + O_{2(g)}$ occurred laggardly behind the reaction of $Ca(ClO)_2 \rightarrow Ca^{2+} + 2Cl^- + O_{2(g)}$ because of its related high Gibbs free energy (Fig. 8 (a)). In the CO_3^{2-} system, the calcium species ($Ca(OH)_2$, Ca^{2+} and $Ca(Cl)_2$) would spontaneously transform into $CaCO_3$, and it was the ultimate dominant calcium species because the Gibbs free energies of corresponding chemical reactions were negative (Fig. 8 (b)). Previous studies indicated that the adsorption of $CaCO_3$ speciation on the pyrite surface was an important factor for the inhibition of pyrite flotation (Ai et al., 2015). On the basis of thermodynamic calculation results, the pyrite surface will be suffered a deepness oxidation in the flotation solution with the addition of $Ca(ClO)_2$ and influx of air. On the one hand, multitude hydrophilic iron oxide ($FeSO_4$, Fe_2O_3 or Fe_3O_4) were generated on the pyrite surfaces due to the strong oxidation of $Ca(ClO)_2$ and oxygen. On the other hand, calcium ions species ($Ca(OH)_2$ and Ca^{2+}) and $CaCO_3$ speciation were formed, which further improve the hydrophilicity of the pyrite surface after the interaction between calcium species and the mineral surface.

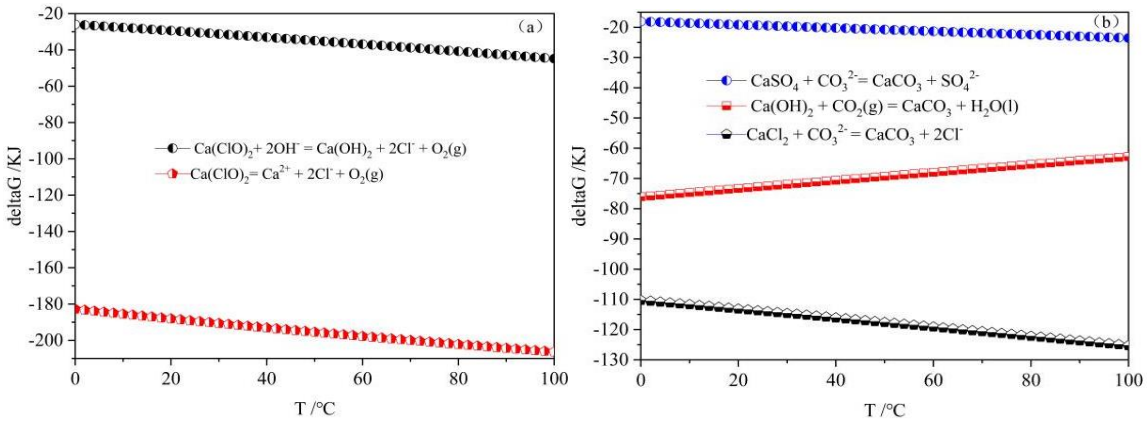

Fig. 8. Relationships between the Gibbs free energy of calcium species transformation reaction and temperature

3.3. DFT simulation of H_2O-$CaCO_3$ adsorption on Fe_2S (100) surface

Based on the experimental evidence of this work, the $CaCO_3$ was the ultimate dominant calcium species after series chemical reactions in the low-alkaline system with combined depressants. The interaction between H_2O-$CaCO_3$ and pyrite surface could reveal the $CaCO_3$ adsorption behavior, and disclose the potential depression mechanism. However, few works were reported on this issue. For clarifying this dimness, DFT simulation calculations were performed. We determined the adsorption energy of H_2O-$CaCO_3$ molecular on the (100) surface of Fe_2S, and the most stable configuration was shown in Fig. 9. The results showed that the Ca atom of $CaCO_3$ and the S atoms on the pyrite surface formed two Ca-S bonds with bond lengths of 2.970 and 2.900 Å, respectively. The O atom of $CaCO_3$ could bond with the Fe and S atoms on the pyrite surface (O2-Fe2, O1-Fe2 and O1-S1) with bond lengths of 2.589, 2.008 and 1.771Å, respectively. This confirmed that the interaction between O atoms of $CaCO_3$ and the Fe atoms on the pyrite was more powerful than corresponding interaction of other atoms, which played a more important role in the adsorption of $CaCO_3$ molecular on the pyrite surface. Besides, the H atom of H_2O and the S atom on the pyrite surface formed H-S bonds with the bond length of 2.670 Å. It could be inferred that the adsorption of H_2O reinforced the hydrophilicity of pyrite surface. Additionally, the calculated adsorption energy of H_2O-$CaCO_3$ molecular on the pyrite surface (ΔE_{ads}) was –671.13 kJ/mol. This negative value confirmed chemical adsorption occurred between H_2O-$CaCO_3$ molecular and surface of pyrite.

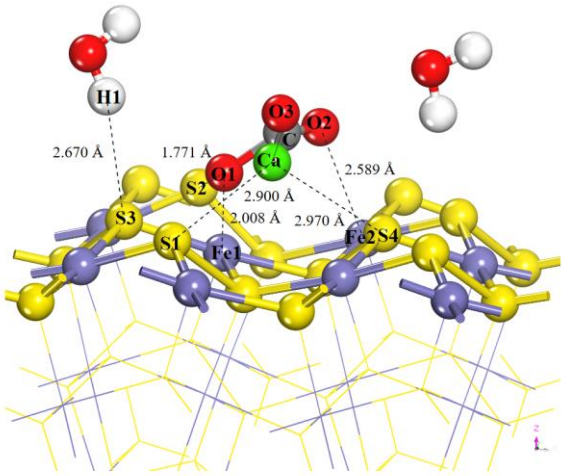

Fig. 9. The optimized configuration of the surface supercell after H_2O-$CaCO_3$ interaction with the FeS_2 (100) surface

The density of states (DOS) profiles of relevant atoms of pyrite surface before and after the H_2O-$CaCO_3$ adsorption were depicted in Fig. 10. The DOS of the Fe1 atoms of pyrite surface at the Fermi

level was composed of s and p energy levels, but the contribution of the p energy level was much larger than that of the s energy level. While, the DOS of the Fe atoms of pyrite surface at the Fermi level was mainly contributed by the d energy level. The DOS of the Fe1 atom on the pyrite (100) surface changed after the H_2O-$CaCO_3$ adsorption. Specially, the Fe1 d peak near the Fermi level became smoother and the number of Fe1 d energy-level peaks decreased. Meanwhile, the Fe1 p peak intensity decreased considerably at the Fermi level, demonstrating that Fe atoms of pyrite surface become less active after the H_2O-$CaCO_3$ adsorption. Whereas, the changes in the DOS of the S1 atom on the pyrite (100) surface before and after the H_2O-$CaCO_3$ adsorption were inconspicuous. This result further confirmed the strong interaction between O atoms of $CaCO_3$ and the Fe atoms on the pyrite occurred.

The DOS of the Ca atom on $CaCO_3$ changed after interacting with pyrite. The Ca d peak intensity increased, and the DOS of Ca d shifted in the direction of higher energy. Similar phenomenon was observed for the DOS of Ca s and Ca p. These results indicated Ca atom on $CaCO_3$ adsorbed onto pyrite surface, bonding with S atoms of pyrite (Ca-S, as depicted in Fig.9). For the DOS of O1 atom after H_2O-$CaCO_3$ adsorption, the O1 p energy-level peak splited into multiple energy-level peaks at -10 to -2 eV, and shifted in the direction of lower energy significantly. Similar phenomenon was observed for the DOS of O1 s. These results indicated O atom on $CaCO_3$ adsorbed onto pyrite surface, bonding with S and Fe atoms of pyrite (O-S and O-Fe as depicted in Fig.9). Given these results, the O1 and Ca atoms mainly contributed to the bonding process and were responsible for the stable adsorption of $CaCO_3$ on the pyrite surface.

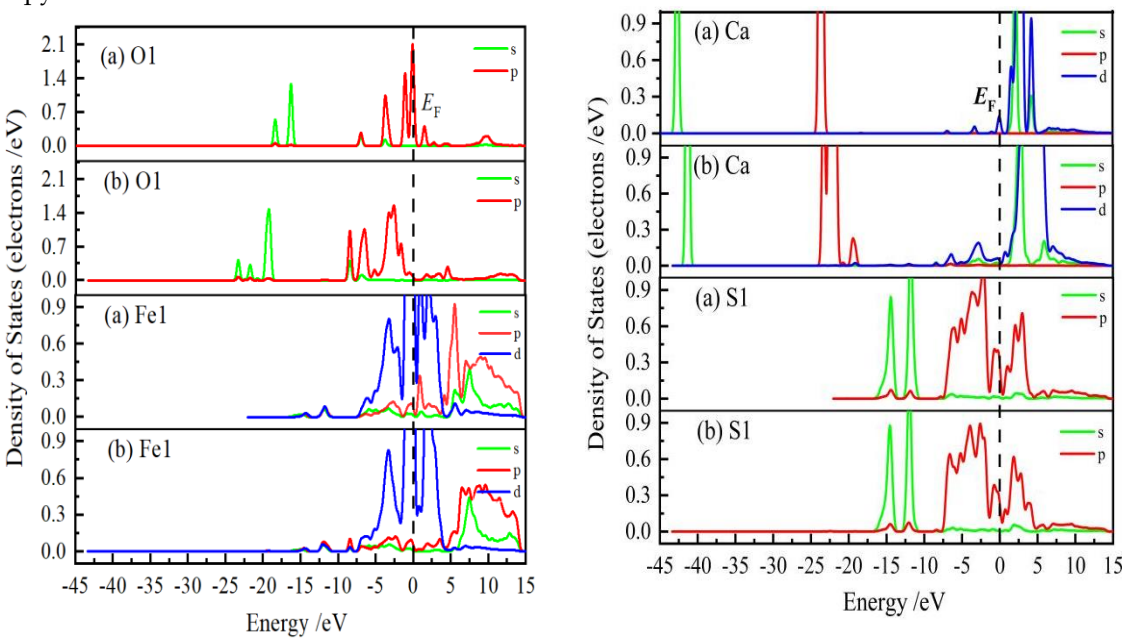

Fig. 10. Density of states of relevant atoms of pyrite (100) surface before (a) and after (b) H_2O-$CaCO_3$ adsorption

The structure of the pyrite (100) surface and the DOS of the atoms were affected by the adsorption of H_2O-$CaCO_3$. The electrical properties of the atoms were also influenced. Therefore, the charge-density differences of the pyrite (100) surface after H_2O-$CaCO_3$ adsorption, and the charge transfer and distribution of bonded atoms before and after H_2O-$CaCO_3$ adsorption on the pyrite (011) surface were investigated. The results were shown in Fig. 11 and Table 1. As shown in Fig.11. The charge density was lower near the Fe atom, and it was an electron-poor region comparing with the corresponding charge density of pyrite other body atoms (as the circled part). Combined with the data in Table 1, the charge of the Fe1 atom increased from 0.07 e to 0.12 e, and the charge of the O1 atom decreased from -0.51 e to -0.61 e, indicating that the electrons lost by the Fe1 atom transferred to the O1 atom, resulting in the electron density of the Fe1 atom decreasing and the formation of Fe1-O1 bond. This activity promoted the oxidation of iron components of pyrite surface. Meanwhile, the charge of the S1 atom decreased from -0.10 e to -0.23 e, and the charge of the Ca atom changed from 1.13 e to 1.31 e. The result indicated that the Ca atom interacted with S atom intensively and contributed to the formation of Ca-S bond.

Thus, $CaCO_3$ could chemically adsorb onto the pyrite surface and increased the hydrophilicity of mineral surfaces.

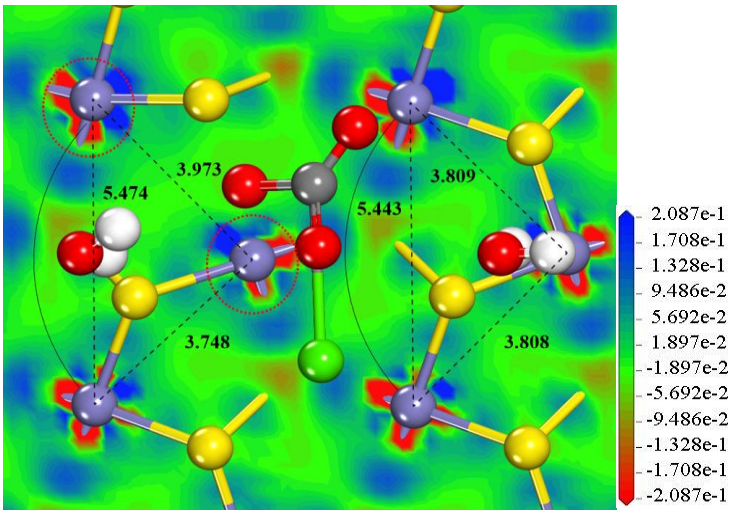

Fig. 11. Charge-density differences of the pyrite (100) surface after H_2O-$CaCO_3$ adsorption. The O, H, S, Fe, C and Ca atoms are displayed as red, white, yellow, lightgray, gray, and green, respectively

Table 1. Mulliken populations of main atoms on the pyrite (100) surface before (a) and after (b) H_2O-$CaCO_3$ adsorption

Atoms		s	p	d	Total electron	Charge (e)
Ca1	(a)	2.51	6.00	0.37	8.87	1.13
	(b)	2.10	5.99	0.60	8.69	1.31
O1	(a)	1.92	4.59	-	6.51	-0.51
	(b)	1.79	4.82	-	6.61	-0.61
S1	(a)	1.86	4.25	-	6.10	-0.10
	(b)	1.84	4.39	-	6.23	-0.23
Fe1	(a)	0.35	0.45	7.12	7.93	0.07
	(b)	0.34	0.50	7.04	7.88	0.12

3.4. ToF-SIMS study

3.4.1. Normalized peak intensities of pyrite samples

With the aim of directly investigate the adsorption characteristics of combined depressants and KBX collector on the pyrite surface, normalized peak intensities from the positive (+) ion ToF-SIMS analysis of pyrite samples before and after treatments of reagents were conducted. As shown in Fig. 12, the normalized peak intensity of $FeOH^+$, $CaOH^+$ and $CaCO^+$ increased, whereas the normalized peak intensity of Fe^+ and $C_4H_9^+$ decreased significantly when the pyrite sample was treated with combined depressants and KBX collector. According to the mass signal of fragments, it could be concluded that the hydrophilic species were in the form of hydroxy calcium, iron carbonyl and calcium carbonate in the presence of combined depressants. Moreover, semiquantitative of hydrophilic species was in the following order: hydroxy calcium>iron carbonyl>calcium carbonate. These findings indicated that the addition of combined depressants increased the formation of hydrophilic species on the pyrite surfaces due to the oxidation of $Ca(ClO)_2$ and the adsorption of calcium components. Besides, the formation of hydrophilic species would wrap on the pyrite surface and well accounted for the remarkable decrease in the normalized peak intensity of Fe^+. As we known, the hydrophobic dixanthogen stemming from the oxidation of xanthates are responsible for the hydrophobization of the pyrite surface (Yang et al., 2018). Herein, the mass signal of $C_4H_9^+$ were mainly fragments of the dixanthogen. The considerably decrease in normalized peak intensity of $C_4H_9^+$ indicated that the combined depressants hindered the

dixanthogen adsorption on the pyrite surfaces due to the formation of hydrophilic sites on the surface, which was the main reason of the decrease in pyrite flotation recovery. Thus, the above results provided strong evidence for the depression of the pyrite flotation through addition of the combined depressants.

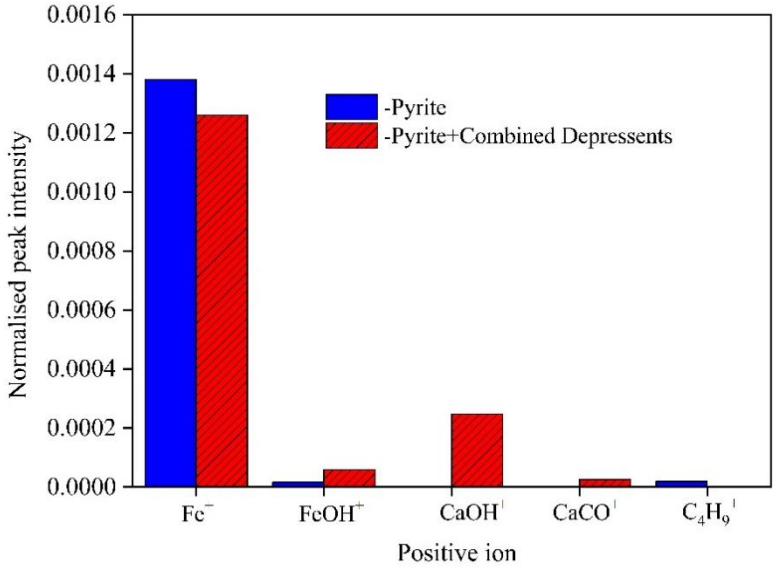

Fig. 12. Normalized peak intensities from the positive ion ToF-SIMS analyses of the pyrite samples before and after treatments of reagents. Conditions: pH = 9.5, 200 mg/L combined depressants (if present) with a mass ratio of CaO to $Ca(ClO)_2$ of 2:3 and 1.0×10^{-3} mol/L KBX.

3.4.2. Three-dimensional (3D) secondary ion images

In order to visualize the spatial variation of the distribution of interested substances on the surface layer of pyrite samples before and after treatments of reagents. 3D secondary ion images were reconstructed (Fig. 13). As indicated in Fig. 13, Fe^+, $FeOH^+$, $CaOH^+$, $CaCO^+$ and $C_4H_9^+$ ions images illustrated the heterogeneous distribution. The $C_4H_9^+$ ions were present on the topmost pyrite surface layer with a few nanometers thick, and facilitated the floatability of the pyrite. For the pyrite sample after treatments of combined depressants, the whole thickness of the formed hydrophilic species ($FeOH^+$, $CaOH^+$, and $CaCO^+$), which was responsible for the depression of the pyrite flotation, was approximately 50 nm. Also, the thickness and abundance of hydrophilic species increased obviously compared with the corresponding results of pyrite sample before combined depressants treatments. Furthermore, the distribution of $C_4H_9^+$ ions on the surface of the pyrite was much thinner than that without the addition of combined depressants. Hence, the distribution of the interest ion species with the addition of combined depressants depressed the floatability of the pyrite.

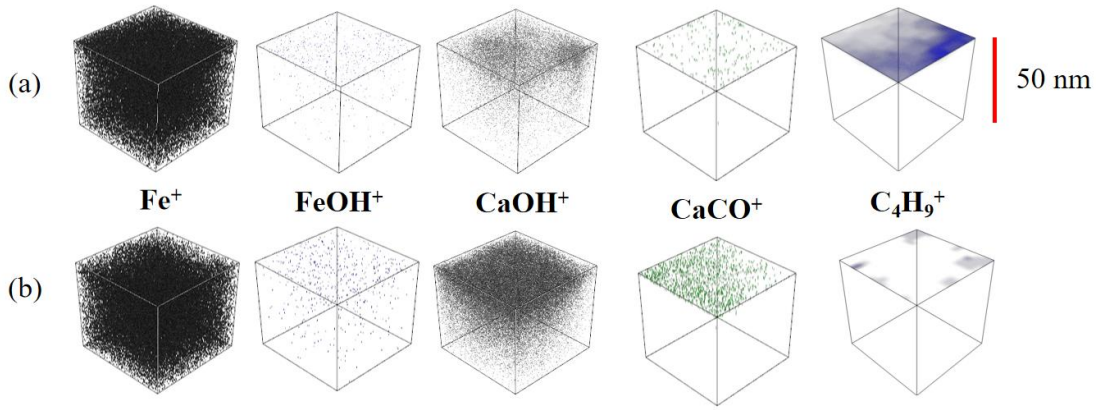

Fig. 13. ToF-SIMS-3D positive ion images of pyrite samples before and after treatments of reagents. Conditions: pH = 9.5, 200 mg/L combined depressants (if present) with a mass ratio of CaO to $Ca(ClO)_2$ of 2:3 and 1.0×10^{-3} mol/L KBX

Along with the aforementioned results and discussion, we constructed a schematic of the depression mechanism on pyrite caused by combined depressants. As shown in Fig. 14, part of iron carbonyl was formed on the pyrite surface during the air flow agitation processing in the Na_2CO_3 system (pH=9.5), and the adsorption of hydrophobic dixanthogen realized the good flotation of pyrite. When the combined depressants ($Ca(ClO)_2$ and CaO) and KBX were added sequentially, the $Ca(ClO)_2$ firstly oxidized the pyrite surfaces, and the hydrophilic calcium components adsorbed onto the mineral surface, result in the cover of multitude hydrophilic species on the pyrite surfaces. This activity repulsed the adsorption of dixanthogen to acquire the poor flotation of pyrite. The hydrophilic species were mainly in the form of hydroxy calcium, iron carbonyl and calcium carbonate. Semiquantitative amounts of hydrophilic species followed the order of hydroxy calcium>iron carbonyl>calcium carbonate. As a result, the floatability of pyrite remarkably decreased.

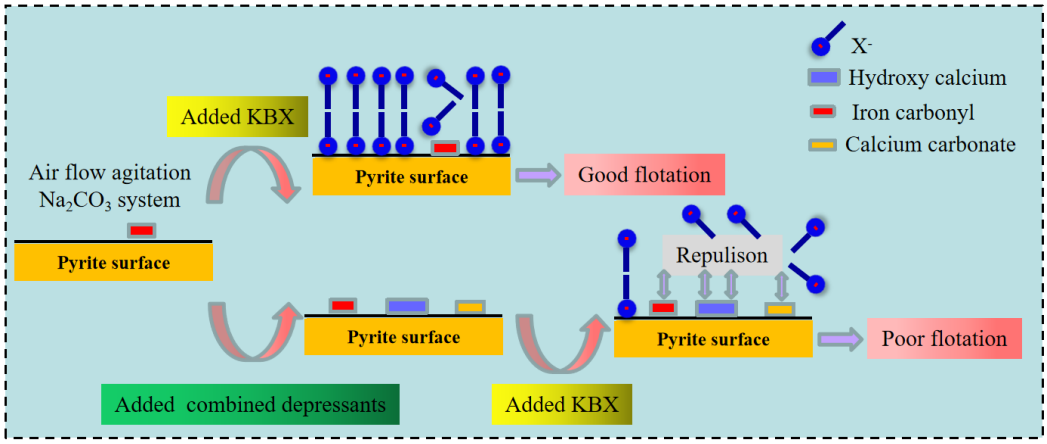

Fig. 14. Schematic representation of the depression mechanism on pyrite caused by combined depressants with air flow agitation in a low-alkaline system

4. Conclusions

Micro-flotation experiments indicate that the addition of 200 mg/L combined depressants (a mass ratios of CaO to $Ca(ClO)_2$ of 2:3) and 1.0×10^{-3} mol/L KBX at pH 9.5 can effectively depress the flotation of pyrite, and a minimum pyrite recovery rate of 12.5% is obtained. Basic thermodynamic evaluation results indicate the participation of $Ca(ClO)_2$ significantly decrease the negative Gibbs free energies of pyrite oxidation reaction. Besides, the calcium species ($Ca(OH)_2$, Ca^{2+} and $Ca(Cl)_2$) will spontaneously transform into $CaCO_3$, and it is the ultimate dominant calcium species in the CO_3^{2-} system. DFT results indicate that $CaCO_3$ can chemically adsorb onto the pyrite surface with an adsorption energy of –671.13 kJ/mol. The O1 and Ca atoms mainly contribute to the bonding process and are responsible for the stable adsorption of $CaCO_3$ on the pyrite surface. ToF-SIMS results provide strong evidence for an increase in the amount of hydrophilic species and a decrease in dixanthogen adsorption onto the surface of the pyrite with the addition of combined depressants. The thickness of the formed hydrophilic species is approximately 50 nm. The hydrophilic species are mainly in the form of hydroxy calcium, iron carbonyl and calcium carbonate. Semiquantitative amounts of hydrophilic species follow the order of hydroxy calcium>iron carbonyl>calcium carbonate. As a result, the hydrophilic species repulse the adsorption of dixanthogen, and the flotation performance of the pyrite remarkably decreases. Results elucidate the depression of pyrite in a low alkaline system with the addition of combined depressants, and thus present a theoretical basis for the selective flotation separation of pyrite from other sulfides. However, the effects of combined depressants on the flotation behaviours of sulfide minerals, such as chalcopyrite, galena and sphalerite require further investigation with aims of high efficiency separation of polymetallic sulphide ore.

Acknowledgment

We would appreciate the Regions of the National Natural Science Foundation of China (Grant No.52164021) and the Natural Science Foundation of Yunnan Province (Grant No. 2019FB078) for

providing financial supports for this research project. We also thanks to the work unit for providing special funds for this research project (Grant No. CCC21321119A).

References

AHMADI, A.,RANJBAR, M. ,SCHAFFIE, M. 2012. *Catalytic effect of pyrite on the leaching of chalcopyrite concentrates in chemical, biological and electrobiochemical systems*. Minerals Engineering. 34, 11-18

AI, G.,ZHOU, Y. ,WANG, Y. 2015. *A Study on the Combined Depressant for the Cu-S Separation in Low Alkaline Medium and its Depressing Mechanism*. Procedia Engineering. 102, 338-345

BAI, S.,BI, Y.,LI, J.,YU, P.,DING, Z.,LV, C. ,WEN, S. 2021. *Innovative utilization of acid mine drainage (AMD): A promising activator for pyrite flotation once depressed in a high alkali solution (HAS)–Gearing towards a cleaner production concept of copper sulfide ore*. Minerals Engineering. 170,

BAI, S.,WEN, S.,XIAN, Y.,LIU, J. ,DENG, J. 2013. *New source of unavoidable ions in galena flotation pulp: Components released from fluid inclusions*. Minerals Engineering. 45, 94-99

BAI, S.,YU, P.,LI, C.,WEN, S. ,DING, Z. 2019. *Depression of pyrite in a low-alkaline medium with added calcium hypochlorite: Experiment, visual MINTEQ models, XPS, and ToF–SIMS studies*. Minerals Engineering. 141,

BARKER, G.J.,GERSON, A.R. ,MENUGE, J.F. 2014. *The impact of iron sulfide on lead recovery at the giant Navan Zn–Pb orebody, Ireland*. International Journal of Mineral Processing. 128, 16-24

BONNISSEL-GISSINGER, P.,ALNOT, M.,EHRHARDT, J.J. ,BEHRA, P. 1998. *Surface Oxidation of Pyrite as a Function of pH*. Environ.sci.technol. 32(19), 2839-2845

BULUT, G.,YENIAL, Ü.,EMIROĞLU, E. ,SIRKECI, A.A. 2014. *Arsenic removal from aqueous solution using pyrite*. Journal of Cleaner Production. 84, 526-532

BUNKHOLT, I. ,KLEIV, R.A. 2015. *Flotation of pyrrhotite and pyrite in saturated CaCO3 solution using a quaternary amine collector*. Minerals Engineering. 70, 55-63

CHANDRA, A.P. ,GERSON, A.R. 2010. *The mechanisms of pyrite oxidation and leaching: A fundamental perspective*. Surface Science Reports. 65(9), 293-315

CHEN, J.,LI, Y. ,CHEN, Y. 2011. *Cu–S flotation separation via the combination of sodium humate and lime in a low pH medium*. Minerals Engineering. 24(1), 58-63

DENG, J.,WEN, S.,XIAN, Y.,LIU, J. ,BAI, S. 2013. *New discovery of unavoidable ions source in chalcopyrite flotation pulp: Fluid inclusions*. Minerals Engineering. 42, 22-28

DICHMANN, T.K. ,FINCH, J.A. 2001. *The role of copper ions in sphalerite-pyrite flotation selectivity*.

DING, Z.,BI, Y.,LI, J.,YUAN, J.,DAI, H. ,BAI, S. 2022. *Flotation separation of chalcopyrite and pyrite via Fenton oxidation modification in a low alkaline acid mine drainage (AMD) system*. Minerals Engineering. 187,

EKMEKCI, Z. ,DEMIREL, H. 1997. *Effects of galvanic interaction on collectorless flotation behaviour of chalcopyrite and pyrite*. International Journal of Mineral Processing. 52(1), 31-48

FERREIRA, H.M.,LOPES, E.B.,MALTA, J.F.,FERREIRA, L.M.,CASIMIRO, M.H.,SANTOS, L.F.,PEREIRA, M.F.C.,MOçO, D. ,GONçALVES, A.P. 2021. *Preparation and densification of bulk pyrite, FeS2*. Journal of Physics and Chemistry of Solids. 159,

FINKELSTEIN, N.P. 1997. *Addendum to: The activation of sulphide minerals for flotation: A review*. International Journal of Mineral Processing. 55(4), 81-120

GUO, B.,PENG, Y. ,PARKER, G. 2016. *Electrochemical and spectroscopic studies of pyrite–cyanide interactions in relation to the depression of pyrite flotation*. Minerals Engineering. 92, 78-85

HUANG, P.,CAO, M. ,LIU, Q. 2013. *Selective depression of pyrite with chitosan in Pb–Fe sulfide flotation*. Minerals Engineering. 46-47, 45-51

HUNG, A.,MUSCAT, J.,YAROVSKY, I. ,RUSSO, S.P. 2002. *Density-functional theory studies of pyrite FeS2(1 0 0) and (1 1 0) surfaces*. Surface Science. 513(3), 511-524

JANETSKI, N.D.,WOODBURN, S.I. ,WOODS, R. 1977. *An electrochemical investigation of pyrite flotation and depression*. International Journal of Mineral Processing. 4(3), 227-239

JIANG, K.,LIU, J.,WANG, Y.,ZHANG, D. ,HAN, Y. 2023. *Surface properties and flotation inhibition mechanism of air oxidation on pyrite and arsenopyrite*. Applied Surface Science. 610,

JIN, S.,SHI, Q.,FENG, Q.,ZHANG, G. ,CHANG, Z. 2018. *The role of calcium and carbonate ions in the separation of pyrite and talc*. Minerals Engineering. 119, 205-211

KHOSO, S.A.,HU, Y.-H.,LÜ, F.,GAO, Y.,LIU, R.-Q. ,SUN, W. 2019. *Xanthate interaction and flotation separation of H2O2-treated chalcopyrite and pyrite*. Transactions of Nonferrous Metals Society of China. 29(12), 2604-2614

LI, Y.,CHEN, J.,KANG, D. ,GUO, J. 2012. *Depression of pyrite in alkaline medium and its subsequent activation by copper*. Minerals Engineering. 26, 64-69

LIAO, R.-P.,HU, P.-J.,WEN, S.-M.,ZHENG, Y.-X.,QIU, X.-H.,LÜ, J.-F. ,LIU, J. 2022. *Interaction mechanism of ferrate(VI) with arsenopyrite surface and its effect on flotation separation of chalcopyrite from arsenopyrite*. Transactions of Nonferrous Metals Society of China. 32(11), 3731-3743

LIU, R.,GUO, Y.,WANG, L.,SUN, W.,TAO, H. ,HU, Y. 2015. *Effect of calcium hypochlorite on the flotation separation of galena and jamesonite in high-alkali systems*. Minerals Engineering. 84, 8-14

L6PEZ VALDIVIESO, A.,CELED6N CERVANTES, T.,SONG, S.,ROBLEDO CABRERA, A. ,LASKOWSKI, J.S. 2004. *Dextrin as a non-toxic depressant for pyrite in flotation with xanthates as collector*. Minerals Engineering. 17(9-10), 1001-1006

MKHONTO, P.P.,ZHANG, X.,LU, L.,XIONG, W.,ZHU, Y.,HAN, L. ,NGOEPE, P.E. 2022. *Adsorption mechanisms and effects of thiocarbamate collectors in the separation of chalcopyrite from pyrite minerals: DFT and experimental studies*. Minerals Engineering. 176,

MU, Y.,PENG, Y. ,LAUTEN, R.A. 2016a. *The depression of pyrite in selective flotation by different reagent systems – A Literature review*. Minerals Engineering. 96-97, 143-156

MU, Y.,PENG, Y. ,LAUTEN, R.A. 2016b. *The mechanism of pyrite depression at acidic pH by lignosulfonate-based biopolymers with different molecular compositions*. Minerals Engineering. 92, 37-46

PECINA, E.T.,URIBE, A.,NAVA, F. ,FINCH, J.A. 2006. *The role of copper and lead in the activation of pyrite in xanthate and non-xanthate systems*. Minerals Engineering. 19(2), 172-179

PENG, Y.,WANG, B. ,GERSON, A. 2012. *The effect of electrochemical potential on the activation of pyrite by copper and lead ions during grinding*. International Journal of Mineral Processing. 102-103, 141-149

SHEN, W.Z.,FORNASIERO, D. ,RALSTON, J. 1998. *Effect of collectors, conditioning pH and gases in the separation of sphalerite from pyrite*. Minerals Engineering. 11(2), 145-158

WANG, X.H. ,FORSSBERG, K. 2002. *Mechanisms of pyrite flotation with xanthates*. International Journal of Mineral Processing. 33(1-4), 275-290

WANG, Z.-J.,XU, L.-H.,WU, H.-Q.,ZHOU, H.,MENG, J.-P.,HUO, X.-M. ,HUANG, L.-Y. 2021. *Adsorption of octanohydroxamic acid at fluorite surface in presence of calcite species*. Transactions of Nonferrous Metals Society of China. 31(12), 3891-3904

WANG, Z.,QIAN, Y.,XU, L.-H.,DAI, B.,XIAO, J.-H. ,FU, K. 2015. *Selective chalcopyrite flotation from pyrite with glycerine-xanthate as depressant*. Minerals Engineering. 74, 86-90

YANG, X.,BORIS, A.,LIU, G. ,ZHOU, Y. 2018. *Structure–activity relationship of xanthates with different hydrophobic groups in the flotation of pyrite*. Minerals Engineering. 125, 155-164

YIN, W.,YANG, B.,FU, Y.,CHU, F.,YAO, J.,CAO, S. ,ZHU, Z. 2019. *Effect of calcium hypochlorite on flotation separation of covellite and pyrite*. Powder Technology. 343, 578-585

ZANIN, M.,LAMBERT, H. ,DU PLESSIS, C.A. 2019. *Lime use and functionality in sulphide mineral flotation: A review*. Minerals Engineering. 143,

ZHANG, Q.,WEN, S.,ZUO, Q. ,FENG, Q. 2023. *Density functional theory calculation of catalytic sulfidization on the azurite (0 1 1) surface by ammonium salts and its effect on flotation*. Separation and Purification Technology. 309,

ZHANG, R.,ZHUO, J.,MAO, Y.,WAN, Q. ,ZHAO, H. 2022. *Effects of different inorganic oxidizers on removal of xanthate pre-adsorbed on chalcopyrite surface: An effective approach for flotation depression using KMnO4*. Minerals Engineering. 184,

ZHAO, G.,FANG, X. ,ZHANG, Y. 2023. *Selective flotation of pyrite from serpentine using phytic acid as the depressant*. Colloids and Surfaces A: Physicochemical and Engineering Aspects. 658,